2021

Transient flow boiling and maldistribution characteristics in heated parallel channels induced by flow regime oscillations

T.A. Kingston

B.D. Olson

J.A. Weibel

S.V. Garimella

Kingston, T.A.; Olson, B.D.; Weibel, J.A.; and Garimella, S.V., "Transient flow boiling and maldistribution characteristics in heated parallel channels induced by flow regime oscillations" (2021). *CTRC Research Publications.* Paper 381.
http://dx.doi.org/10.1109/TCPMT.2021.3106226

Transient Flow Boiling and Maldistribution Characteristics in Heated Parallel Channels Induced by Flow Regime Oscillations

Todd A. Kingston, Brian D. Olson, Justin A. Weibel, and Suresh V. Garimella

***Abstract*—Flow boiling provides an effective means of heat removal but can suffer from thermal and hydrodynamic transients that compromise heat transfer performance and trigger device failure. In this study, the transient flow boiling characteristics in two thermally isolated, hydrodynamically coupled parallel microchannels are investigated experimentally. High-speed flow visualization is synchronized to high-frequency heat flux, wall temperature, pressure drop, and mass flux measurements to provide time-resolved characterization. Two constant and two transient heating conditions are presented. For a constant heat flux of 63 kW/m^2 into each channel, boiling occurs continuously in both channels and the parallel channel instability is observed to occur at 15 Hz. Time-periodic oscillations in the pressure drop and average mass flux are observed, but corresponding oscillations in the wall temperatures are virtually non-existent at this condition. At a slightly lower constant heat flux of 60 kW/m^2, boiling remains continuous in one of the channels, but the other channel experiences time-periodic flow regime oscillations between single-phase and two-phase flow. At this condition, extreme time-periodic wall temperature oscillations are observed in both channels with a long period (~7 s) due to oscillations in the severity of the flow maldistribution. For the transient heating conditions, square wave heating profiles oscillating between different heat flux levels are applied to the channels. Because of their relatively high frequency, the heating transients are attenuated by the microchannel walls, resulting in effectively constant heating conditions and flow boiling characteristics like that of the aforementioned constant heating conditions. This study illustrates the susceptibility of parallel two-phase heat sinks to flow maldistribution, particularly when undergoing transient flow regime oscillations.**

***Index Terms*—Flow boiling, flow regime, flow maldistribution, flow instability, parallel microchannels, transient heating, two-phase flow.**

NOMENCLATURE

c_p	Specific heat.
D	Microchannel inside diameter.
G_{avg}	Average microchannel mass flux.
h_{fg}	Heat of vaporization.
k	Thermal conductivity.
Δp	Pressure drop across the test section.
p_{in}	Pressure at inlet plenum.
p_{out}	Pressure at outlet plenum.
P_{net}	Net power into each microchannel.
P_{loss}	Power loss to ambient.
P_{total}	Total power applied.
L_{heated}	Heated length of each microchannel.
t	Time.
T	Temperature.
T_{sat}	Saturation temperature.
T_{wall}	Microchannel outside wall temperature.
V	Voltage.
I	Current.
Q	Volumetric flow rate.
q_{net}	Net heat flux into each microchannel.
z	Axial position along the heated length of each microchannel.

Greek letters

μ	Dynamic viscosity.
ρ	Density.
σ	Surface tension.

I. INTRODUCTION

FLOW boiling is an attractive thermal management strategy for the dissipation of high heat fluxes because of the high heat transfer coefficients achievable with the evaporating flow as well as the potential to maintain low pumping powers if operated at high exit vapor quality. The dissipation of extreme die-level heat fluxes in excess of 1000 W/cm^2 using dielectric fluids, a longstanding objective in the field [1, 2], can be achieved by implementing 'embedded cooling' strategies where the coolant is routed directly through the device [3-5]. However, despite this significant potential, two-phase flows often suffer from flow instabilities and flow maldistribution, which can lead to the occurrence of critical heat flux at levels

This research was sponsored by the Naval Engineering Education Consortium (NEEC), with support of Naval Surface Warfare Center (NSWC) Crane Division in Crane, Indiana. (*Corresponding author: Justin A. Weibel*)

T.A. Kingston is with the Center for Multiphase Flow Research and Education, Department of Mechanical Engineering, Iowa State University, Ames, Iowa 50011, USA (e-mail: kingston@iastate.edu).

B.D. Olson is with the Naval Surface Warfare Center Crane Division, Crane, Indiana 47522, USA (e-mail: brian.d.olson1@navy.mil)

J.A. Weibel is with the Cooling Technologies Research Center, School of Mechanical Engineering, Purdue University, West Lafayette, Indiana 47907, USA (e-mail: jaweibel@purdue.edu)

S.V. Garimella is with the University of Vermont, Burlington, Vermont 05405, USA (e-mail: sureshg@purdue.edu)

This paper has supplementary downloadable multimedia material provided by the authors available online. This includes corresponding videos of the synchronized flow visualization and sensor measurements for each figure presented in the Results and Discussion section (Fig. 2 - Fig. 5).

well below theoretical predictions [6, 7]. Moreover, self-sustained hydrodynamic and thermal oscillations often observed in two-phase systems can have significant repercussions and even cause device failure. This is of particular concern for embedded cooling architectures where the coolant is very close to the heat generation source. These thermal oscillations can not only lead to a reduction in device lifetime but, in some instances, also compromise device functionality. For example, consider multifunctional coherent radar systems, which often feature solid-state power amplifiers (*e.g.*, GaAs or GaN) and rely on transmitting time interleaved coherent processing interval (CPI) waveform sequences to execute several simultaneous functions (*e.g.*, surveillance, tracking, etc.). These CPI waveforms can require different amounts of power from the amplifiers, which induces transients in the power amplifier's self-heating characteristics from one CPI to the next. Testing has shown that multifunctional operation often results in changes to amplitude gain and insertion phase as a result of electrothermal 'memory' effects [8, 9]. In other words, the operational characteristics of the radar are temperature-dependent, and thermal transients (either self-induced or externally enforced by a cooling system) on the timescale of the CPIs can diminish device functionality.

Flow boiling instabilities continue to be extensively studied because of their potential impact on two-phase cooling performance. Several reviews on flow boiling instabilities are available [10, 11], including the seminal review by Boure et al. [6] and a recent review by O'Neill and Mudawar [12]. These reviews highlight the instability types and mechanisms and summarize recent advancements. Two classes of flow instabilities have been identified, static and dynamic. Static instabilities are often identified as events that cause a departure from one unstable operating condition to another. These include critical heat flux, or the sudden thermal excursion that often results in failure, and others of interest such as the Ledinegg instability and the flow pattern transition instability. In contrast, dynamic instabilities, such as the pressure drop instability or parallel channel instability, feature inertial and feedback effects that cause time-periodic oscillations. It is worth noting that while some instability types are classified as static instabilities, they may manifest in a dynamic instability mode [12]. For example, the flow regime transition instability (a static instability), which features transitions between different flow regimes (*e.g.*, bubbly and slug), often occurs cyclically.

The types of instabilities observed are often dependent on system design and operation. For example, the introduction of an inlet restrictor [13-15] at the entrance of a microchannel, or artifical nucleation sites along the microchannel [16, 17], has been shown to decrease the severity of thermal and hydrodynamic oscillations. Studies that intentionally isolate various system components/parameters and provide time-resolved characterization of the instability mechanisms and their implications have benefited our understanding. For example, Huh et al. [18] used a microchannel fabricated from polydimethylsiloxane (PDMS) with an array of microheaters/temperature sensors to study the cyclic flow pattern transition instability in a single channel. However, many times these instability mitigation/isolation techniques are not achievable in practice, and additional or superimposed flow boiling instabilities need to be considered. For instance, flow boiling in parallel heat sinks or channels (versus a serial arrangement) is often necessary to distribute the coolant. From servers in data centers to the transmit/receive modules in phased array radar systems, coolant must be routed through parallel piping networks to the locations of the heat sources. The typical thermal isolation between the individual heat sinks in these applications makes the flow boiling process even more susceptible to flow maldistribution and temperature oscillations, since the lack of thermal coupling prevents heat from being redistributed between heat sinks. Van Oevelen *et al*. [19] modeled the steady-state two-phase flow distribution in a large number of thermally isolated parallel channels for a wide range of operating parameters and showed that the Ledinegg instability [20] resulted in severe flow maldistribution that reduced significantly with thermal coupling [21]. Flynn *et al.* [22, 23] investigated the hydrodynamic interactions and thermal implications of flow boiling in two parallel channels under both thermally isolated and coupled configurations. In both configurations, uniform heating of the channels caused either single-phase or two-phase flow through both channels and a minimal time-averaged temperature difference was observed. However, in the thermally isolated configuration, non-uniform heating of the channels caused boiling in one of the channels and flow maldistribution; a large time-averaged channel-to-channel temperature difference in the downstream half of the channels was reported.

Time-resolved characterization of hydrodynamic and thermal oscillations in parallel channel configurations, as previously explored in single-channel studies, is required to improve our understanding of the instability types and their implications on thermal performance. In this study, we use high-speed flow visualizations and high-frequency sensor measurements under both constant and transient heating conditions to investigate the transient flow boiling characteristics in two hydrodynamically coupled, thermally isolated parallel channels. Time-varying thermal and hydrodynamic oscillations that result from the flow characteristics are reported and their implications are discussed.

II. Experimental Methods

A. Test Facility

The experimental facility illustrated in Fig. 1a is modified from our previous single-channel study [24] to enable characterization of the flow boiling process in parallel microchannels. The facility uses a pressurized reservoir to deliver degassed, dielectric HFE-7100 (Novec Engineered Fluid, 3M; fluid properties listed in Table I) to two parallel channels; the pressure difference between the reservoir and the ambient is used to generate an open-loop flow. A cartridge heater (G6A-15568, Watlow) is suspended inside the reservoir and supplied with electric power using an adjustable direct current (DC) power supply (XG 850W 150-5.6, Sorensen), which boils the fluid inside the rigid stainless steel reservoir and

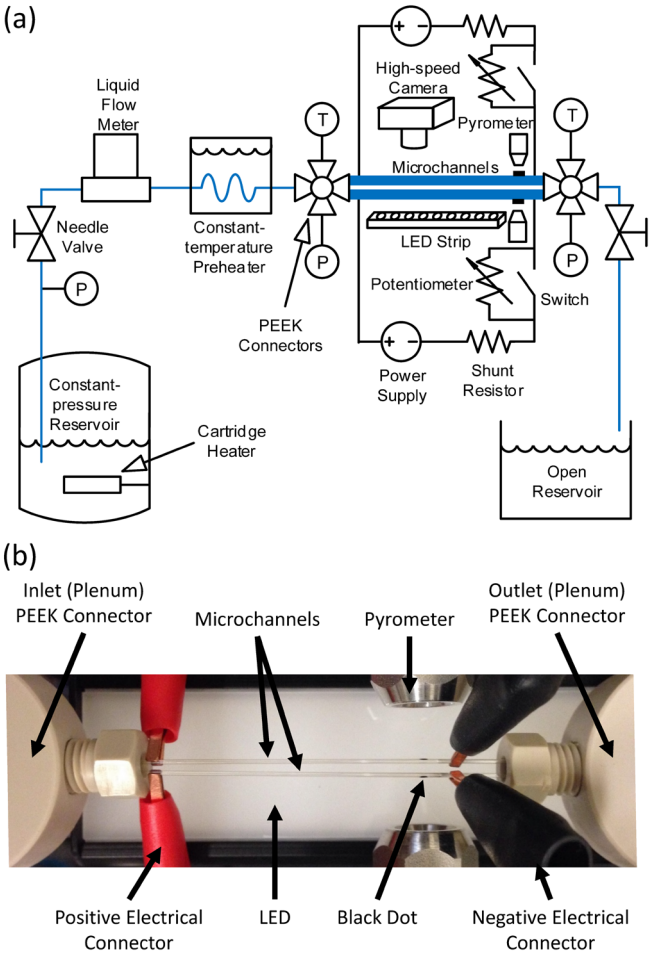

Fig. 1. (a) Schematic diagram of the experimental test facility and (b) a photograph of the test section.

maintains a constant reservoir pressure throughout testing.

Liquid HFE-7100 is fed from the reservoir via an internal dip tube. The liquid flow rate and the pressure at the outlet plenum of the test section are set using a pair of needle valves (FVL-404-SS and FVL-405-SS, Omega Engineering), one upstream and one downstream of the test section, respectively. The volumetric flow rate and temperature of the liquid are measured using a flow meter which also features an internal temperature sensor (LC-10CCM-D-EPDM, Alicat; accuracy of ± 1% full scale). Incoming liquid is preheated immediately upstream of the inlet plenum by passing it through a constant-temperature circulating bath (NESLAB EX 17, Thermo Electron Corp.).

Fluid inlet and outlet connections to the test section are mounted to polyetheretherketone (PEEK) connectors (ZX2LPK, Valco Instruments). The temperature and pressure of the fluid in these inlet and outlet plenums (*i.e.*, entering and exiting the channels) are respectively measured using small thermocouples (TMTSS-020E-6, Omega Engineering; ± 0.5 °C) and two separate pressure transducers (PX309-030G5V and PX309-015G5V, Omega Engineering; ± 1%).

TABLE I
FLUID PROPERTIES OF SATURATED HFE-7100 AT ATMOSPHERIC PRESSURE [25]

	Liquid	Vapor
Density, ρ [kg/m^3]	1399	9.87
Specific heat, c_p [J/(kg °C)]	1255	929
Thermal conductivity, k [W/(m K)]	0.0618	0.0156
Dynamic viscosity, μ [kg/(m s)]	3.61×10^{-4}	1.12×10^{-5}
Heat of vaporization, h_{fg} [J/kg]	— 111600 —	
Saturation temperature, T_{sat} [°C]	—— 61 ——	
Surface tension, σ [N/m]	— 0.0103 —	

Two nominally identical, circular cross-section, parallel microchannels made of borosilicate glass (CV5070, VitroCom) with an inside diameter of D = 500 ± 3 μm and a wall thickness of 100 μm are horizontally mounted side-by-side in between the inlet and outlet plenum (Fig. 1b). The outside periphery of the microchannels is custom-coated with a nominally 100 nm-thick layer of indium tin oxide (ITO), which is optically transparent and electrically conductive, thereby enabling visualization of the two-phase flow simultaneous with Joule heating. Electric power is independently supplied to each ITO coating using two adjustable DC power supplies (XG 850W 300V-2.8A, Sorensen; accuracy of ± 0.5%). A solid-state switch (PAA140, IXYS Corp.) and several potentiometers (RJS10KE, RHS1K0E, RES100E; Ohmite) placed in series with each power supply allow the power to be switched between two different levels. The switch is activated by a high-frequency data acquisition (DAQ) unit (USB-6259, National Instruments) that is controlled using LabVIEW. Electrically insulating polytetrafluoroethylene (PTFE) ferrules and PEEK nuts connect the ITO-coated microchannels to the PEEK inlet and outlet plenums.

Outside wall (channel) temperatures are noninvasively measured at a single fixed location on each microchannel using two separate pyrometers (CTfast LT25F, Optris; accuracy of ± 2 °C) and focusing lenses (ACCTCF, Optris). Each pyrometer is focused on a small black dot applied to the outside surface of each channel using a high-temperature paint. The heated length of each channel is L_{heated} = 42 mm and the axial position of the wall temperature measurement is near the downstream end of this heated length at (z / L_{heated}) = 0.90. The heated region is visualized from the top using a high-speed camera (VEO710L, Phantom) and a macro lens (AF Micro-Nikkor, Nikon) using an image resolution of 1280 × 88 at 2500 fps. A light-emitting diode (LED) strip with an integrated light diffuser (BL168, Advanced Illumination) is placed below the channels to provide uniform backlighting. High-speed optical images are synchronized to heat flux, wall temperature, pressure drop, and average mass flux measurements, all of which are recorded at 2.5 kHz, using a pulse generator (565, Berkeley Nucleonics Corp.), which simultaneously triggers the camera and DAQ unit. The test facility is mounted on a damped optical table (VIS3672-PG2-325A, Newport Corp.) to eliminate external vibrations.

B. Test Procedure

Immediately prior to testing, the working fluid was degassed by vigorously boiling the liquid in the reservoir fitted with a Graham condenser using the submerged cartridge heater, as described in Ref. [26]. Non-condensable gases were expelled, while the HFE-7100 vapor was condensed back into the reservoir using an auxiliary flow loop (not shown in Fig. 1). While degassing, the working fluid was also circulated through

another auxiliary flow loop (also not shown in Fig. 1) featuring a 2 μm particulate filter (SS-4TF-2, Swagelok) and an activated-carbon filter (12011 Pall Corporation) to remove any contaminants.

Experiments commenced by boiling the liquid in the reservoir until a constant reservoir pressure of 190 kPa was reached. Liquid flow through the test section was then initiated and the needle valves were adjusted such that an average mass flux of 400 kg/m^{2}s through the channels and a saturation pressure (temperature) of 114 kPa (65 °C) at the outlet plenum were achieved. Because the test facility features a constant pressure difference across the system instead of a constant mass flux, the instantaneous mass flux through the system can vary from the initial setting once boiling occurs. Moreover, the flow distribution between the two individual channels can vary, even if the combined time-averaged flow rate through the two channels remains constant. The temperature of the liquid entering the inlet plenum was 60 °C, which corresponds to an inlet liquid subcooling of 5 °C based on the outlet saturation temperature. After achieving the desired flow conditions, electric power was applied to each ITO coating to create either a constant or transient heat flux profile. Once steady or, in the case of boiling conditions, time-periodic conditions were achieved, optical images and sensor data were simultaneously acquired for 45 s.

C. Data Reduction

The voltage output from each pyrometer is converted to a temperature using a calibration, as described in Ref. [27]. A fraction of the total power supplied to each ITO-coated channel is lost to the ambient instead of being transferred to the fluid through the channel wall. This power loss is temperature dependent and was determined using a calibration, as described in Ref. [27]. Due to the thermal isolation between the two parallel microchannels, the power loss of a particular channel is not dependent on the temperature of the other channel. The net power dissipated by the fluid in each channel is determined by subtracting the power loss from the total power supplied using $P_{net} = P_{total} - P_{loss}$. The total power supplied to each channel is calculated using $P_{total} = VI$ where V and I are the voltages applied to and the currents through the ITO coating on each channel.

The net heat flux into the fluid is calculated using $q_{net} = P_{net} / (\pi D L_{heated})$. The average mass flux through the two channels is calculated as $G = Q\rho / (2\pi D^2/4)$ where Q is the measured total volumetric flow rate and ρ is the calculated liquid density corresponding to the measured liquid temperature at the flow meter. The mass flux through each individual channel cannot be resolved by the upstream flow meter, however, inferences about the flow distribution can be made by measuring the difference in the wall temperatures between the two channels during single-phase flow testing. For example, for a constant heat flux of 30 kW/m^2 (the highest heat flux in the single-phase flow regime) applied to each channel, the wall temperatures of channels 1 and 2 were 109 °C and 105 °C, respectively. Based on this small temperature difference, we can infer that the mass fluxes through the two channels are nearly identical and only very minor flow maldistribution due to geometric effects (*e.g.*, channel placement in the inlet and outlet plenums) is present. The pressure drop across the channels is equal and is calculated as the difference between the inlet and outlet plenum pressures, $\Delta p = p_{in} - p_{out}$.

III. Results and Discussion

A. Constant Heating Conditions

1) Parallel Channel Instability During Continuous Boiling

Fig. 2 shows the time-resolved wall temperatures, pressure drop, and average mass flux when both channels are subjected to a constant heat flux of 63 kW/m^2. Below these transient data, images extracted from the flow visualizations of channel 1 (upper channel in the figure) and channel 2 (lower channel) are shown at select time instants. At this operating condition, boiling is occurring continuously in both channels and the parallel channel instability (described in the next paragraph) is observed. Spectral analysis of the pressure drop and average mass flux signals for this test condition via a fast Fourier transform indicates that the characteristic frequency of the parallel channel instability is approximately 15 Hz; this has been corroborated by the flow visualizations. Despite the parallel channel instability-induced hydrodynamic oscillations, wall temperature oscillations do not occur. The wall temperatures of channels 1 and 2 remain relatively constant, at 114 °C and 77 °C, respectively. This channel-to-channel temperature difference is likely the result of maldistribution of the time-averaged flow between the two channels. Because the flow maldistribution was assessed to be very mild during single-phase flow (as described in Section II.C), it is postulated that flow boiling exacerbated the differences in the channel characteristics caused a much larger temperature difference. To explain the relatively constant channel wall temperatures, in our previous work on the effects of transient heating conditions on flow boiling characteristics in a single channel [28], we concluded that transient heating frequencies above 10 Hz were attenuated by the microchannel wall and did not propagate to the fluid. Here, the hydrodynamic oscillations at 15 Hz induced by the parallel channel instability do not translate to thermal oscillations in the channel wall temperatures because they exceed the previously identified cutoff frequency of 10 Hz.

The parallel channel instability observed in many two-phase parallel channel systems is the result of density wave oscillations within each channel and the interactive feedback between the two channels [29]. This instability is characterized by time-periodic oscillations in the vapor front upstream and downstream within each channel, which are out of phase with respect to each other. As shown in Fig. 2, these oscillations in the flow morphology coincide with time-periodic oscillations in the pressure drop and average mass flux. We postulate that the individual mass flux through each channel (which is not measured) is varying significantly with time. As shown in the first (top) flow visualization in Fig. 2 (t = 0.179 s), channel 1 features a continuous vapor core surrounded by a thin liquid film. Meanwhile, liquid is flowing into channel 2 and vapor bubbles are nucleating and departing the microchannel wall at

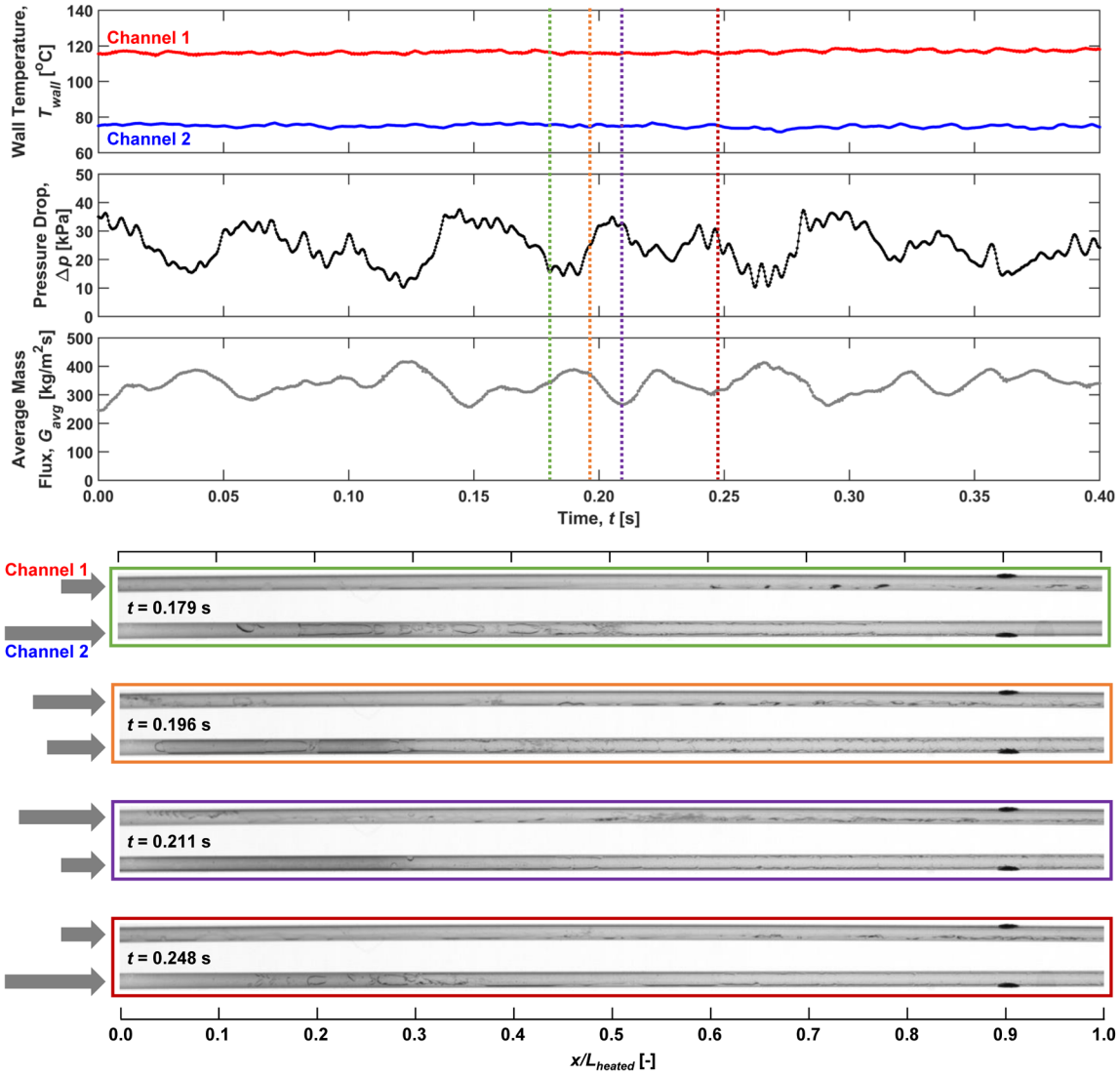

Fig. 2. Synchronized measurements of wall temperatures, pressure drop, and average mass flux as a function of time and selected images of the two-phase morphology when both channels are subjected to a constant heat flux of 63 kW/m^2. The flow direction is from left to right and the black dots on the channel wall near the outlet correspond to the locations of the wall temperature measurements. At this operating condition, boiling is occurring continuously in both channels and the parallel channel instability is observed. A corresponding video of the synchronized flow visualization and sensor measurements is available online in the Supplementary Materials (Video S1).

approximately x/L_{heated} = 0.13. Upon departure, these vapor bubbles flow downstream, grow rapidly due to evaporation, and coalesce to form a continuous vapor core with a thin liquid layer surrounding it beginning at approximately x/L_{heated} = 0.5. At this instant in time (t = 0.179 s), the pressure drop is at a local minimum (16 kPa). Based on the vapor bubble dynamics, we speculate that the mass flux into channel 2 is significantly higher than channel 1. These instantaneous relative flow rates into each of the channels are qualitatively represented by the gray arrows next to the channel inlets in Fig. 2.

At t = 0.196 s, a vapor-liquid mixture enters channel 1 while the vapor front in channel 2 appears to be moving rapidly upstream (indicative of local flow reversal); the pressure drop has increased to 25 kPa. At t = 0.211 s, solely liquid is entering channel 1 and small vapor bubbles are nucleating and departing from the microchannel wall at x/L_{heated} = 0.03. At this same time, channel 2 features a continuous vapor core with a thin liquid layer surrounding it, the pressure drop is near a local maximum (32 kPa), and the average mass flux is at a local minimum (268 kg/m^{2}s). Here, it is inferred that the instantaneous mass flux through channel 1 is higher than that of channel 2. It is worth noting that the overall flow morphology of the test section at t = 0.179 s is similar to that at t = 0.211 s, but with the individual flow morphologies of each channel reversed. Note that the time required for the flow morphologies of the two channels to be interchanged (0.211 s - 0.179 s = 0.032 s) corresponds to approximately 30 Hz, which is twice the characteristic frequency of the parallel channel instability (*i.e.*, ~15 Hz). Thus, it represents one half cycle of the parallel channel instability. These out-of-phase hydrodynamic oscillations in the individual channel flow morphology continue and by t = 0.248 s (fourth frame of the flow visualizations shown in Fig. 2), the flow characteristics of each channel are similar to that at t = 0.179 s (the first frame), with this time period corresponding to the measured oscillation frequency of the parallel channel instability (*i.e.*, 15 Hz).

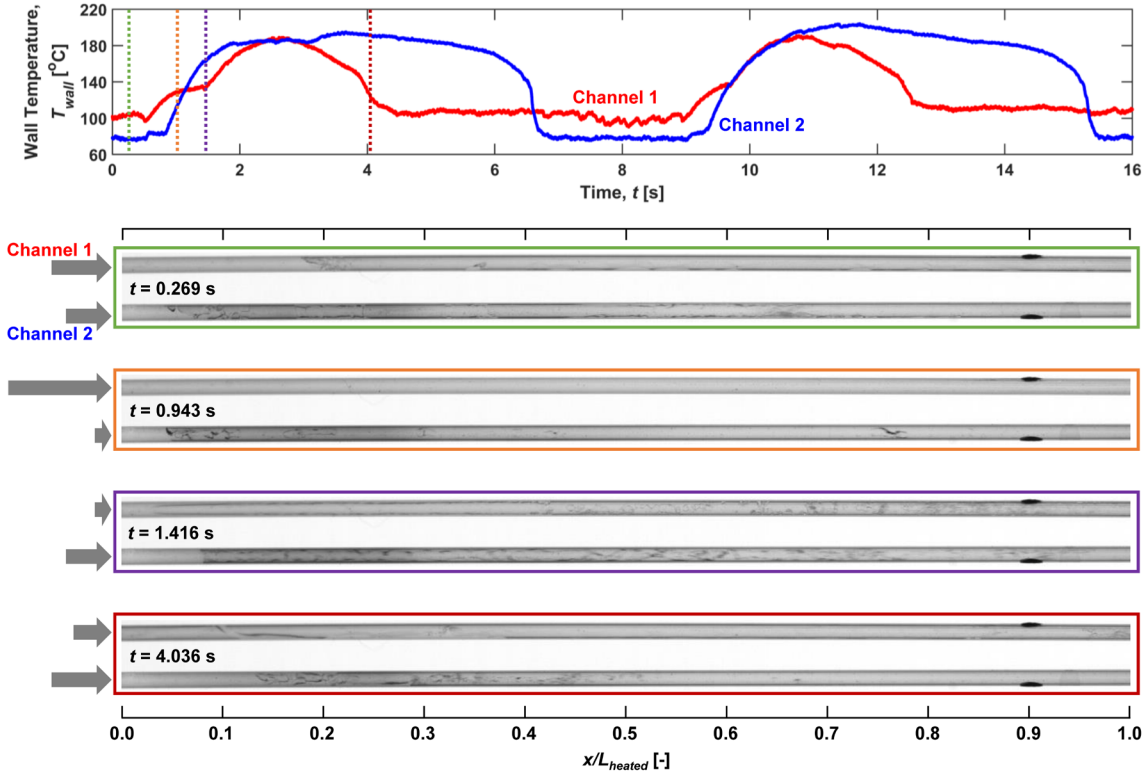

Fig. 3. Time-resolved channel wall temperatures and selected images of the two-phase flow morphology when both channels are subjected to a constant heat flux of 60 kW/m^2. At this operating condition, channel 1 undergoes time-periodic flow regime oscillations between single-phase and two-phase flow and channel 2 features continuous boiling. A corresponding video of the synchronized flow visualization and wall temperature measurements is available online in the Supplementary Materials (Video S2).

2) Time-periodic Flow Regime Oscillations

To investigate the potential impact of flow regime oscillations on transient temperature signatures under constant heating conditions, the heat flux applied to the two channels was intentionally reduced just slightly to 60 kW/m^2. This heat flux level was specifically chosen because it resulted in time-periodic flow regime oscillations between single-phase and two-phase flow in channel 1, while preserving continuous boiling in channel 2. These oscillations are similar to the flow regime transition instability reported in the literature [6, 12], except in this study the flow regime oscillates between single-phase and two-phase flow, instead of between different two-phase flow regimes. Shown in Fig. 3 are the time-resolved channel wall temperatures over a 16 s time period and select images showing the two-phase morphology at specific instants. For this test condition, the hydrodynamic oscillations induce large thermal oscillations not only in channel 1 which sees flow regime oscillations, but also (and with even larger magnitude) in channel 2 where boiling is continuously occurring.

For this test condition, boiling is occurring in both channels from $0 \leq t < 0.493$ s, as indicated in the first flow visualization (t = 0.269 s). During this time period, the parallel channel instability is occurring (with characteristics as described in the previous section). At t = 0.493 s, the vapor front in channel 1 moves completely downstream resulting in single-phase flow in this channel (as shown in the second flow visualization frame). At this instant in time, the wall temperature in channel 1 begins increasing asymptotically, from 99 °C at t = 0.493 s to 136 °C at t = 1.410 s. As a result of the change in the flow morphology in channel 1, the wall temperature of channel 2 begins increasing at t = 0.833 s because the vapor within channel 2 now has a significantly higher flow resistance relative to the single-phase flow in channel 1. Given that boiling is still occurring in channel 2, the rapid rise in wall temperature indicates that the instantaneous heat transfer coefficient is significantly reduced and thus the mass flow is extremely low. We speculate that at this time, the vast majority of the fluid entering the inlet plenum is being routed through channel 1. At t = 1.410 s, the large wall temperature of channel 1 causes a vapor bubble to nucleate from the wall near the outlet of the channel. Because the liquid in channel 1 is likely superheated at this time (based on our previous study of the rapid-bubble-growth instability [26]), the evaporation at the bubble interface is so large that the vapor bubble grows rapidly both upstream and downstream in an explosive-like manner (as shown in the third flow visualization frame in Fig. 3 at t = 1.416 s) until channel 1 is filled with a vapor core and only a thin liquid layer separates it from the channel wall. This local flow reversal within channel 1 impedes incoming liquid and causes fluid to preferentially flow through channel 2. This causes the wall temperature of channel 1 to increase even further to 189 °C at t = 2.615 s and slows the temperature rise of channel 2 and causes it to level off at a maximum of 195 °C at t = 3.662 s. Following the times at which the wall temperatures reach a maximum in both channels, the wall temperatures reduce slowly as time-periodic oscillations in the vapor fronts of each channel associated with the parallel channel instability continue to occur out-of-phase with each

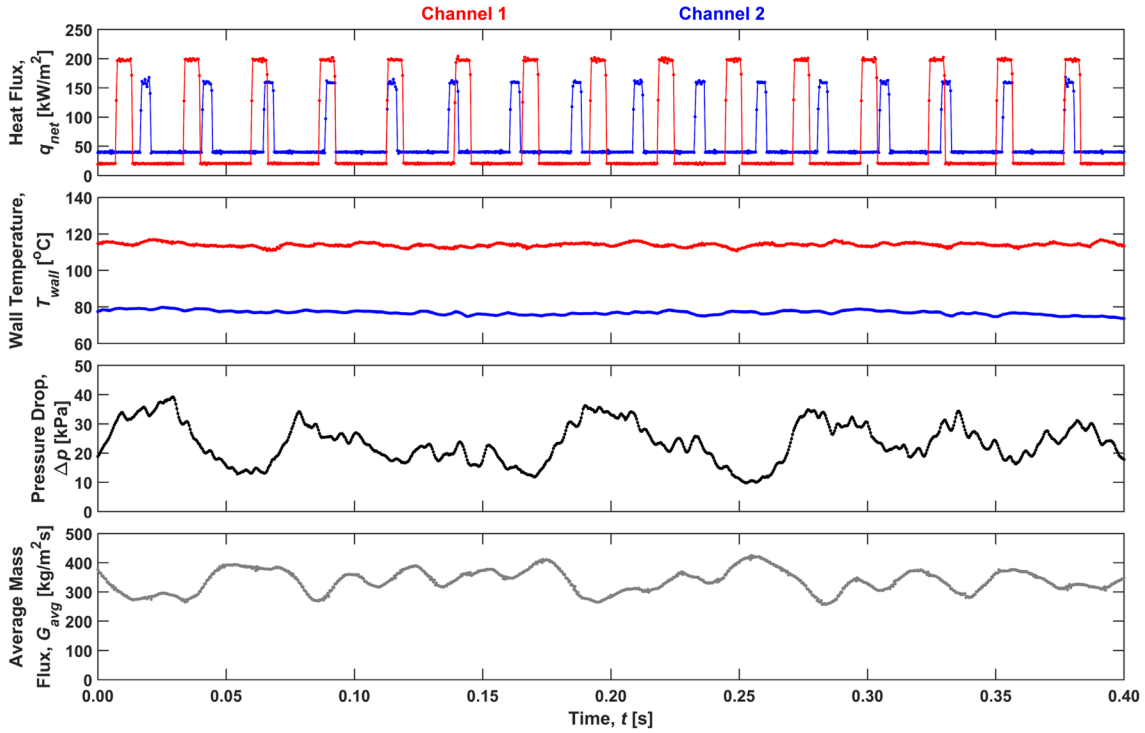

Fig. 4. Time-resolved measurements of heat flux, wall temperatures, pressure drop, and average mass flux when channel 1 is subjected to a heat flux oscillating between 20 kW/m^2 and 200 kW/m^2 at a frequency and duty cycle of 38 Hz and 24%, respectively, and channel 2 is subjected to a heat flux oscillating between 40 kW/m^2 and 160 kW/m^2 at a frequency and duty cycle of 42 Hz and 17%, respectively. If time averaged, the two transient heating profiles for channels 1 and 2 would correspond to heat fluxes of 63 kW/m^2 and 60 kW/m^2, respectively. At this condition, boiling is occurring continuously in both channels and the parallel channel instability is observed. A corresponding video of the synchronized flow visualization and sensor measurements is available online in the Supplementary Materials (Video S3).

other, as shown in the fourth flow visualization frame in Fig. 3 at t = 4.036 s. Only after a relatively long delay, by t ~ 7 s, do the temperatures of the two channels reassume their initial values prior to the flow regime transition to single-phase flow in channel 1. Boiling (and the parallel channel instability) continues in both channels until t = 8.963 s, at which point there is a transition to single-phase flow in channel 1 and the process just described repeats cyclically, as shown by the temperature signatures in Fig. 3 from t = 8.963 - 16 s. A notable takeaway from this experiment is that, despite single-phase flow only being present in channel 1 for a short time (*e.g.*, t = 0.493 - 1.410 s), the thermal effects due to this flow regime transition can persist for much longer (*e.g.*, t = 0.493 to ~ 7 s).

B. Transient Heating Conditions

To probe the potential implications of transient heating conditions on flow boiling characteristics, the operational characteristics of solid-state power amplifiers used by Tua [8] and Tua *et al.* [9] to investigate amplitude and phase transients resulting from self-heating electrothermal 'memory' effects are used in this study to inform the transient heating conditions for the two microchannels. We assume that the CPIs in each sequence result in a constant heat flux to the system's coolant over the interval and the magnitude of the heat flux depends on the duty cycle (good assumptions given the pulse repetition frequency within a CPI is up to thousands of Hertz). In Ref. [8], two successive CPI waveforms (denoted here as CPI_A and CPI_B) had a CPI of 0.0064 s at a duty cycle of 10% and a CPI of 0.020 s at a duty cycle of 1%. Thus, there is a 10:1 ratio in the operating power for these waveforms. For the purposes of this study, we assign a heat flux of 20 kW/m^2 to the lower-power waveform and assume a square wave heating profile oscillating between the two heat flux levels. Therefore, the heat flux profile applied to one of the microchannels oscillates between 20 kW/m^2 and 200 kW/m^2 at an effective frequency of 38 Hz [defined as $1/(CPI_A+CPI_B)$] and duty cycle of 24% [defined as $CPI_A/(CPI_A+CPI_B)$]. As shown in our previous single-channel studies [24, 30], a constant heat flux of 20 kW/m^2 results in single-phase flow while that of 200 kW/m^2 exceeds what would be critical heat flux under constant heating conditions. In Ref. [9], the CPI waveforms had a CPI of 0.004 s at a duty cycle of 8% and a CPI of 0.020 s at a duty cycle of 2%. Therefore, the heat flux applied to the other microchannel in this study oscillates between 40 kW/m^2 and 160 kW/m^2 at an effective frequency and duty cycle of 42 Hz and 17%, respectively. These two transient heating profiles were applied to the two microchannels to study their effect (or lack thereof) on the flow boiling characteristics.

Fig. 4 shows the time-resolved heat flux, wall temperatures, pressure drop, and average mass flux when channel 1 is subjected to the heat flux profile oscillating between 20 kW/m^2 and 200 kW/m^2 and channel 2 is subjected to the heat flux oscillations between 40 kW/m^2 and 160 kW/m^2. At this operating condition, boiling is occurring continuously in both channels. As shown, the time-periodic heat flux pulses do not induce a thermal or hydrodynamic response in the flow boiling process at their heating frequencies. The wall temperatures are virtually unaffected by the short, high-heat-flux pulses and the

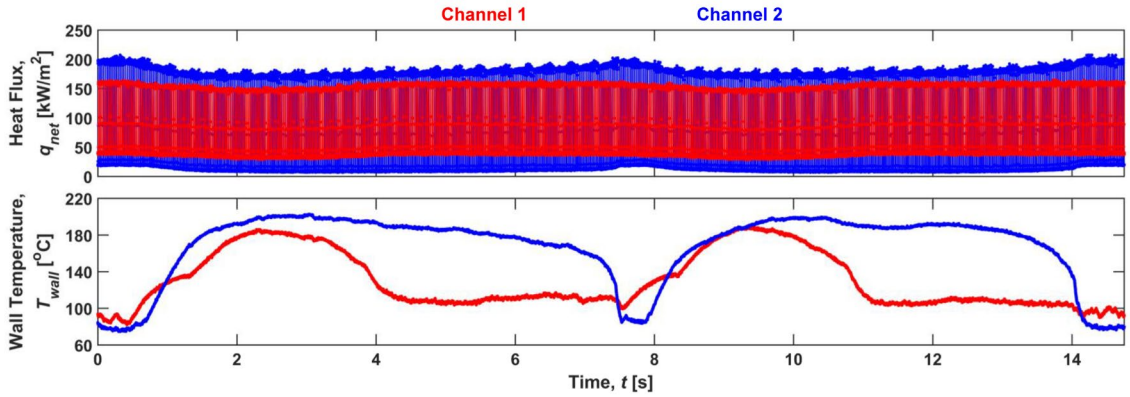

Fig. 5. Transient heat flux and wall temperatures as a function of time when channel 1 is subjected to a heat flux oscillating between 40 kW/m^2 and 160 kW/m^2 at a frequency and duty cycle of 42 Hz and 17%, respectively, and channel 2 is subjected to a heat flux oscillating between 20 kW/m^2 and 200 kW/m^2 at a frequency and duty cycle of 38 Hz and 24%, respectively. If time averaged, the two transient heating profiles for channels 1 and 2 would correspond to heat fluxes of 60 kW/m^2 and 63 kW/m^2, respectively. At this operating condition, channel 1 undergoes time-periodic flow regime oscillations between single-phase and two-phase flow and channel 2 features continuous boiling. A corresponding video of the synchronized flow visualization and wall temperature measurements is available online in the Supplementary Materials (Video S4).

observed hydrodynamic (pressure drop and average mass flux) oscillations result from a parallel channel instability that occurs at approximately 15 Hz. Note that the wall temperatures and amplitude and frequency of the hydrodynamic oscillations are nearly identical to those shown in Fig. 2. This is largely because the time-averaged heat flux into channels 1 and 2 during this operating condition are 63 kW/m^2 and 60 kW/m^2, respectively, and the constant heat flux level corresponding to Fig. 2 was 63 kW/m^2. Based on these observations, we conclude that the transient heat flux pulses are entirely attenuated by the microchannel wall and the channels effectively experience a temporally constant heat flux. This finding in the parallel channel test section is consistent with our previous single-channel study [28].

If the transient heating profiles applied to channels 1 and 2 are interchanged, the flow boiling characteristics are vastly different. This occurs because, despite the fact that the two channels are nominally identical, slight variations in the surface characteristics of the two channels can heavily influence the nucleation behavior and thus the flow boiling process. Shown in Fig. 5 are the transient heat flux and wall temperatures when channel 1 is subjected to the heat flux profile oscillating between 40 kW/m^2 and 160 kW/m^2 and channel 2 is subjected to heat flux profile oscillating between 20 kW/m^2 and 200 kW/m^2. Because the duration of time in Fig. 5 is so large (14.75 s) and the frequency of the heat flux oscillations is relatively high, the square wave heat flux profiles in Fig. 5 overlap and are not distinguishable. Here, the time-averaged heat flux for channels 1 and 2 are 60 kW/m^2 and 63 kW/m^2, respectively. At this operating condition, time-periodic flow regime oscillations between single-phase and two-phase flow are occurring in channel 1 while continuous flow boiling is occurring in channel 2. Comparing the transient heat flux profiles to the wall temperature measurements, it is again obvious that the transient heat flux inputs are not propagating to the fluid, and any thermal oscillations observed at a much longer time scale are caused by other hydrodynamics. In particular, the thermal oscillations look virtually identical to those shown in Fig. 3 and are caused by the same low-frequency flow regime oscillations. The minor reduction in the time-averaged heat flux applied to channel 1 from 63 kW/m^2 to 60 kW/m^2 that induces the large temperature oscillations in this condition again demonstrates the sensitivity of the flow boiling process to these flow regime oscillations (and heat flux level).

IV. Conclusions

This study experimentally investigated the flow boiling characteristics of HFE-7100 in two thermally isolated, hydrodynamically coupled parallel microchannels subjected to constant and transient heating conditions. Flow visualization was synchronized to heat flux, wall temperature, pressure drop, and mass flux measurements to provide time-resolved characterization. For the two constant heating conditions presented, vastly different flow boiling characteristics were observed for a small change in the heat flux applied uniformly to both channels. At a constant heat flux of 63 kW/m^2, continuous boiling occurred in both channels and the parallel channel instability was observed. While time-periodic hydrodynamic oscillations associated with this instability occurring at 15 Hz were observed, wall temperature oscillations were negligible. In contrast, at a slightly reduced constant heat flux of 60 kW/m^2, time-periodic flow regime oscillations between single-phase and two-phase flow with a period of a ~7 s occurred in one channel while continuous flow boiling occurred in the other channel. These flow regime oscillations led to extreme temporal oscillations in the flow maldistribution between the two channels and exacerbated the magnitude of the wall temperature oscillations. Interestingly, the channel experiencing continuous flow boiling consistently had the larger temperature oscillations (between 73 °C to 205 °C), while the temperature oscillations in the channel undergoing the flow regime oscillations were slightly smaller (from 80 °C to 195 °C). The thermal isolation between the two channels prohibited heat exchange between them and exacerbated the transient temperature oscillations. In applications where thermally isolated heat sinks are hydrodynamically connected in parallel, modulation of coolant flow rates to individual heat sinks would be beneficial to maintaining more uniform device

temperatures. The transient heating conditions used in this study were inspired by the operational characteristics of solid-state power amplifiers used in multifunctional radars. Coherent processing interval waveform sequence characteristics such as CPI duration and duty cycle were used as a foundation for a square-wave heating profile oscillating between two distinctly different heat flux levels. Because the frequencies of the heating transients were relatively high (up to 42 Hz), the heat flux oscillations were attenuated by the microchannel wall and effectively resulted in flow behaviors consistent with the constant heating conditions. Overall, this investigation demonstrates the susceptibility of parallel two-phase heat sinks to flow maldistribution, particularly when undergoing transient flow regime oscillations.

REFERENCES

[1] A. Bar-Cohen, "Gen-3 Thermal Management Technology: Role of Microchannels and Nanostructures in an Embedded Cooling Paradigm," *Journal of Nanotechnology in Engineering and Medicine,* vol. 4, no. 2, p. 020907, 2013, doi: 10.1115/1.4023898.

[2] A. Bar-Cohen, J. J. Maurer, and J. G. Felbinger, "DARPA's intra/interchip enhanced cooling (ICECool) program," presented at the Compound Semiconductor Manufacturing Technology Conference, 2013.

[3] K. P. Drummond, D. Back, M. D. Sinanis, D. B. Janes, D. Peroulis, J. A. Weibel, and S. V. Garimella, "Characterization of hierarchical manifold microchannel heat sink arrays under simultaneous background and hotspot heating conditions," *International Journal of Heat and Mass Transfer,* vol. 126, pp. 1289-1301, 2018, doi: 10.1016/j.ijheatmasstransfer.2018.05.127.

[4] R. K. Mandel, D. G. Bae, and M. M. Ohadi, "Embedded two-phase cooling of high flux electronics via press-fit and bonded FEEDS coolers," *Journal of Electronic Packaging,* vol. 140, no. 031003, 2018, doi: 10.1115/1.4039264.

[5] T. Harirchian and S. V. Garimella, "Boiling heat transfer and flow regimes in microchannels - A comprehensive understanding," *Journal of Electronic Packaging,* vol. 133, no. 1, Mar 2011, doi: 10.1115/1.4002721.

[6] J. A. Boure, A. E. Bergles, and L. S. Tong, "Review of two-phase flow instability," *Nuclear Engineering and Design,* vol. 25, no. 2, pp. 165-192, 1973, doi: 10.1016/0029-5493(73)90043-5.

[7] A. E. Bergles and S. G. Kandlikar, "On the nature of critical heat flux in microchannels," *Journal of Heat Transfer,* vol. 127, no. 1, pp. 101-107, Jan 2005, doi: 10.1115/1.1839587.

[8] C. G. Tua, "Measurement technique to assess the impact of RF power amplifier memory effects on radar performance," presented at the IEEE Radar Conference, 2012.

[9] C. G. Tua, T. Pratt, and A. I. Zaghloul, "A study of interpulse instability in gallium nitride power amplifiers in multifunction radars," *IEEE Transactions on Microwave Theory and Techniques,* vol. 64, no. 11, pp. 3732-3747, 2016, doi: 10.1109/tmtt.2016.2604808.

[10] L. Tadrist, "Review on two-phase flow instabilities in narrow spaces," *International Journal of Heat and Fluid Flow,* vol. 28, no. 1, pp. 54-62, 2007, doi: 10.1016/j.ijheatfluidflow.2006.06.004.

[11] S. Kakac and B. Bon, "A review of two-phase flow dynamic instabilities in tube boiling systems," *International Journal of Heat and Mass Transfer,* vol. 51, no. 3-4, pp. 399-433, 2008, doi: 10.1016/j.ijheatmasstransfer.2007.09.026.

[12] L. E. O'Neill and I. Mudawar, "Review of two-phase flow instabilities in macro- and micro-channel systems," *International Journal of Heat and Mass Transfer,* vol. 157, p. 119738, 2020, doi: 10.1016/j.ijheatmasstransfer.2020.119738.

[13] A. Koşar, C. J. Kuo, and Y. Peles, "Suppression of boiling flow oscillations in parallel microchannels by inlet restrictors," *Journal of Heat Transfer,* vol. 128, no. 3, pp. 251-260, 2006, doi: 10.1115/1.2150837.

[14] G. Wang, P. Cheng, and A. E. Bergles, "Effects of inlet/outlet configurations on flow boiling instability in parallel microchannels," *International Journal of Heat and Mass Transfer,* vol. 51, no. 9-10, pp. 2267-2281, 2008, doi: 10.1016/j.ijheatmasstransfer.2007.08.027.

[15] A. Kaya, M. R. Ozdemir, M. Keskinoz, and A. Kosar, "The effects of inlet restriction and tube size on boiling instabilities and detection of resulting premature critical heat flux in microtubes using data analysis," *Applied Thermal Engineering,* vol. 65, no. 1-2, pp. 575-587, Apr 2014, doi: 10.1016/j.applthermaleng.2014.01.062.

[16] S. G. Kandlikar, W. K. Kuan, D. A. Willistein, and J. Borrelli, "Stabilization of flow boiling in microchannels using pressure drop elements and fabricated nucleation sites," *Journal of Heat Transfer,* vol. 128, no. 4, pp. 389-396, Apr 2006, doi: 10.1115/1.2165208.

[17] C. J. Kuo and Y. Peles, "Flow boiling instabilities in microchannels and means for mitigation by reentrant cavities," *Journal of Heat Transfer,* vol. 130, no. 7, p. 072402, 2008, doi: 10.1115/1.2908431.

[18] C. Huh, J. Kim, and M. H. Kim, "Flow pattern transition instability during flow boiling in a single microchannel," *International Journal of Heat and Mass Transfer,* vol. 50, no. 5-6, pp. 1049-1060, 2007, doi: 10.1016/j.ijheatmasstransfer.2006.07.027.

[19] T. Van Oevelen, J. A. Weibel, and S. V. Garimella, "Predicting two-phase flow distribution and stability in systems with many parallel heated channels," *International Journal of Heat and Mass Transfer,* vol. 107, pp. 557-571, 2017, doi: 10.1016/j.ijheatmasstransfer.2016.11.050.

[20] M. Ledinegg, "Instability of flow during natural and forced circulation," *Die Warme,* vol. 61, no. 8, pp. 891-898, 1938.

[21] T. Van Oevelen, J. A. Weibel, and S. V. Garimella, "The effect of lateral thermal coupling between parallel microchannels on two-phase flow distribution," *International Journal of Heat and Mass Transfer,* vol. 124, pp. 769-781, 2018, doi: 10.1016/j.ijheatmasstransfer.2018.03.073.

[22] R. D. Flynn, D. W. Fogg, J.-M. Koo, C.-H. Cheng, and K. E. Goodson, "Boiling flow interaction between two parallel microchannels," presented at the ASME International Mechanical Engineering Congress and Exposition, 2006.

[23] R. Flynn, C.-H. Cheng, and K. Goodson, "Decoupled thermal and fluidic effects on hotspot cooling in a boiling flow microchannel heat sink," presented at the ASME International Technical Conference and Exhibition on Packaging and Integration of Electronic and Photonic Microsystems, 2007.

[24] T. A. Kingston, J. A. Weibel, and S. V. Garimella, "Time-resolved characterization of microchannel flow boiling during transient heating: Part 1 - Dynamic response to a single heat flux pulse," *International Journal of Heat and Mass Transfer,* vol. 154, no. 119643, 2020, doi: 10.1016/j.ijheatmasstransfer.2020.119643.

[25] 3M. 3M Novec Engineered Fluid HFE-7100 for Heat Transfer, St. Paul, MN, 2002.

[26] T. A. Kingston, J. A. Weibel, and S. V. Garimella, "High-frequency thermal-fluidic characterization of dynamic microchannel flow boiling instabilities: Part 1 – Rapid-bubble-growth instability at the onset of boiling," *International Journal of Multiphase Flow,* vol. 106, pp. 179-188, 2018, doi: 10.1016/j.ijmultiphaseflow.2018.05.007.

[27] T. A. Kingston, J. A. Weibel, and S. V. Garimella, "Ledinegg instability-induced temperature excursion between thermally isolated, heated parallel microchannels," *International Journal of Heat and Mass Transfer,* vol. 132, pp. 550-556, 2019, doi: 10.1016/j.ijheatmasstransfer.2018.12.017.

[28] T. A. Kingston, J. A. Weibel, and S. V. Garimella, "Time-resolved characterization of microchannel flow boiling during transient heating: Part 2 - Dynamic response to time-periodic heat flux pulses," *International Journal of Heat and Mass Transfer,* vol. 154, no. 119686, 2020, doi: 10.1016/j.ijheatmasstransfer.2020.119686.

[29] W. Qu and I. Mudawar, "Measurement and prediction of pressure drop in two-phase micro-channel heat sinks," *International Journal of Heat and Mass Transfer,* vol. 46, no. 15, pp. 2737-2753, 2003, doi: 10.1016/s0017-9310(03)00044-9.

[30] T. A. Kingston, J. A. Weibel, and S. V. Garimella, "High-frequency thermal-fluidic characterization of dynamic microchannel flow boiling instabilities: Part 2 – Impact of operating conditions on instability type and severity," *International Journal of Multiphase Flow,* vol. 106, pp. 189-201, 2018, doi: 10.1016/j.ijmultiphaseflow.2018.05.001.

Todd A. Kingston is an Assistant Professor in the Department of Mechanical Engineering at Iowa State University. He received a Ph.D. degree in 2019 from Purdue University and M.S. and B.S. degrees from Iowa State University in 2013 and 2011, respectively, all in Mechanical Engineering. His research interests include multiphase thermal-fluid transport, thermal management, energy transfer and conversion, boiling heat transfer, and thermo-electrochemical coupling phenomena.

Brian D. Olson is the Solid-State Technologies Chief Engineer for the Radar Division at Naval Surface Warfare Center (NSWC) Crane. He received his Ph.D., M.S., and B.E. all in Electrical Engineering from Vanderbilt University in 2010, 2006, and 2003, respectively. His interests are in radio frequency (RF) transmit/receive modules, RF sub-components, amplifiers, and semiconductor technology.

Justin A. Weibel is a Research Associate Professor in the School of Mechanical Engineering at Purdue University and Director of the Cooling Technologies Research Center (CTRC), a graduated NSF I/UCRC. He received his PhD in 2012 and BSME in 2007, both from Purdue University. Dr. Weibel's research explores methodologies for prediction and control of heat transport to enhance the performance and efficiency of thermal management technologies and energy transfer processes. Dr. Weibel has supervised over 30 PhD and MS students and co-authored over 140 referred journal and conference papers. He was recently recognized as an Outstanding Engineering Teacher by the College of Engineering at Purdue University and received the 2020 ASME Electronic & Photonic Packaging Division (EPPD) Young Engineer Award. He is an Associate Editor of the IEEE Transactions on Components Packaging and Manufacturing Technology.

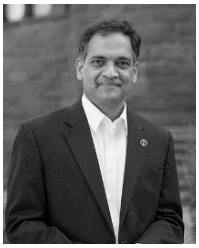

Suresh V. Garimella is President of the University of Vermont (UVM), Professor in the Department of Mechanical Engineering at UVM, and Distinguished Professor Emeritus of Mechanical Engineering at Purdue University, where he founded the National Science Foundation Cooling Technologies Research Center. He has supervised over 90 Ph.D. and M.S. students, has co-authored 600 refereed journal and conference publications, and holds 13 patents. Twenty-eight alumni from his research group are now faculty members at prestigious universities around the world. His research group has made seminal contributions to micro and nanoscale thermal and fluidic engineering, novel materials for thermal management, materials processing and manufacturing, and renewable energy. Dr. Garimella is a Member of the National Science Board (NSB) and Fellow of the National Academy of Inventors, and of AAAS and ASME. His contributions to thermal management have been recognized with the 2016 ITherm Achievement Award, 2010 Heat Transfer Memorial Award, and 2009 Allan Kraus Thermal Management Medal.